Fabrication of a novel and green thin-film composite membrane containing nanovoids for water purification

Zhe Yang[a], Xiaoyu Huang[a], Xiao-hua Ma[a,c], Zhi-wen Zhou[b], Hao Guo[a], Zhikan Yao[a], Shien-Ping Feng[b], Chuyang Y. Tang[a*]

[a] Department of Civil Engineering, the University of Hong Kong, Pokfulam, Hong Kong

[b] Department of Mechanical Engineering, the University of Hong Kong, Pokfulam, Hong Kong

[c] School of Chemical Engineering, East China University of Science and Technology, Mei Long Road 130, Shanghai 200237, P. R. China

[*] To whom all correspondence should be addressed.

Tel: +852 2859 1976, Fax: +852 2559 5337, E-mail address: tangc@hku.hk

Abstract

Thin film nanocomposite (TFN) membranes, which incorporate nanomaterials in a crosslinked polyamide matrix, often show enhanced separation properties thanks to the additional pores or channels offered by these materials. In this study, we deliberately created nanovoids in the dense polyamide rejection layer by acid-etching copper nanoparticles (CuNPs) contained in a TFN membrane. Systematic membrane characterization confirmed the complete removal of CuNPs using 1% HNO_3, which formed nanovoids of approximately 10 nm in size. The water flux of the etched membrane TFC-Cu50X was nearly quadrupled compared to that of the CuNPs loaded membrane TFC-Cu50. This significantly improved water flux can be ascribed to the enhanced water transport through these nano-sized voids. The nanovoids-enhanced approach provides new possibilities for synthesizing high performance membranes.

Keywords: Thin-film composite membrane; polyamide rejection layer; copper nanoparticles; nanovoids; water permeability

Graphical abstract

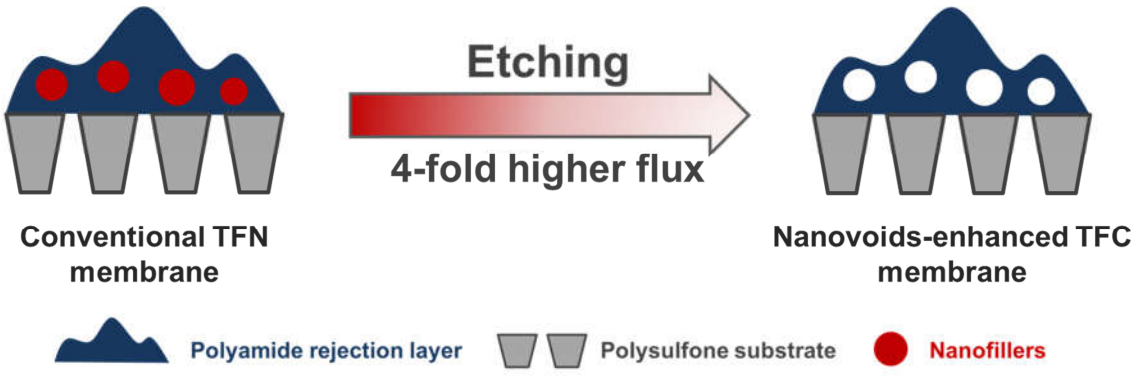

1. Introduction

Thin-film nanocomposite (TFN) membranes, which incorporate nanomaterials in a salt-rejecting polyamide (PA) layer, have attracted tremendous attention in the past decade [1-3]. Compared to thin-film composite (TFC) membranes, TFN can dramatically improve membrane water permeability (e.g., up to 200% enhancement), while maintaining similar salt rejection [1]. Notably, the embedded nanomaterials with micro or mesopores, such as zeolite [4, 5], mesoporous silica [6, 7], metal-organic-framework (MOF) [8] and carbon nanotubes [9] could further enhance membrane water permeability compared to their solid counterparts. The higher water flux can be ascribed to the preferential water pathway in the nanovoids of these porous nanomaterials [6]. Despite the enhanced membrane separation performance, conventional TFN membranes still have some obstacles, such as potential leaching [10] and nanomaterials toxicity [11].

The improved porosity of polyamide rejection layer can significantly improve membrane separation performance [12, 13]. As an alternative approach to conventional TFN, Livingston and co-workers [14] applied microporous monomers for interfacial polymerization, resulting in the formation of a microporous cross-linked rejection layer that showed excellent permeability and selectivity compared to commercial membranes. In a more recent study [13], we reported series of approaches to generate nanovoids in the polyamide rejection layer by the formation

of nanosized gas bubbles (e.g., by the addition of bicarbonate or ultrasound application) during the interfacial polymerization. These nanovoids significantly increased both membrane water permeability and salt rejection. Several studies also highlighted the importance of the microporous structure of membrane rejection layer [15-20].

In this study, we report a facile method to fabricate novel high performance TFC membranes, where nanovoids were generated through the etching of nanoparticles incorporated in the PA-PSF interface. Specifically, we first synthesized copper nanoparticles (CuNPs) loaded TFN membranes, followed by their removal using an HNO_3 solution to create an "arch-like" polyamide morphology. We hypothesize that these nanovoids could significantly decrease the membrane hydraulic resistance, thus greatly enhancing water permeability. This work provides a novel insight into the fabrication of a high performance nanovoids-enhanced TFC membrane.

2. Methods

2.1. Materials and reagents

Chemicals for the preparation of membrane substrates and interfacial polymerization, including polysulfone (PSF, Mw 35,000), *N,N*-dimethylformamide (DMF, anhydrous 99.8%), *m*-Phenylenediamine (MPD, flakes, 99%), trimesoyl chloride (TMC, 98%), and hexane (HPLC grade, 97%) were all obtained from Sigma-Aldrich. Cupric sulfate-anhydrous ($CuSO_4$, AR, Dieckmann, Hong Kong) and sodium borohydride ($NaBH_4$, 98%, Sigma-Aldrich) were used to generate CuNPs *in situ* on polysulfone substrate. Sodium chloride (NaCl) was obtained from Uni-Chem, and nitric acid (HNO_3, 69%) was provided by VWR Chemicals (Dorset, U.K.).

2.2. Synthesis of PSF and CuNPs functionalized PSF support layers

The polysulfone support layer (15 wt. % in DMF) were prepared based on our previous study [21]. The recipe of copper nanoparticles (CuNPs) coating is modified from the literature [22]. As shown in Fig. 1, a polysulfone substrate membrane (20 × 12 cm) was placed in a container. A 50 mL $CuSO_4$ solution was poured onto the polysulfone substrate for 10 mins under continuous shaking of 50 revolutions per minute (rpm) on a reciprocal shaking bath (Unitronic Reciprocal 6032011, J.P. Selecta, S.A., Barcelona, Spain). The excess $CuSO_4$ solution was removed by a rubber roller before. A 50 mL $NaBH_4$ solution was poured onto the $CuSO_4$ impregnated polysulfone substrate for 5 mins under the same shaking condition to form the copper nanoparticles. After that, the resulting substrate was rinsed for approximately 5 mins

with deionized (DI) water. Based on the concentration (0, 50, 100, 200mM) of the $CuSO_4$ and $NaBH_4$ solutions, the CuNPs coated polysulfone substrates are denoted as PSF, PSF-Cu50, PSF-Cu100, and PSF-Cu200, respectively.

2.3. Synthesis of TFC and, TFC-Cu and TFC-CuX membranes

To prepare polyamide rejection layer on the polysulfone substrate, we performed interfacial polymerization on the PSF-Cu substrates (Fig. 1). Briefly, a PSF-Cu substrate was immersed in a 1.0 wt. % MPD-water solution for 3 mins. Then, the excess MPD/water solution was removed by a rubber roller. A TMC-hexane solution (0.2 wt. %) was then added onto the MPD impregnated substrate for 1 min to form the polyamide rejection layer. The resultant membrane was immediately rinsed with hexane and stored in an oven at 60℃ for 10 mins. Finally, the obtained membrane was stored in DI water at least overnight before use. The control TFC membrane was directly synthesized on the PSF substrate without CuNPs treatment. The resultant membranes are named as TFC, TFC-Cu50, TFC-Cu100 and TFC-Cu200 membranes, respectively, based on their CuNPs loading conditions.

To generate nanovoids in the polyamide layer, we etched the CuNPs in the TFC-Cu membranes (Fig. 1). Briefly, a TFC-Cu membrane was immersed in a 1 % HNO_3 solution for 1 day with continuous shaking (50 rpm) to wash away these copper nanoparticles. These etched membranes are denoted as TFC-Cu50X, TFC-Cu100X and TFC-Cu200X, respectively. In addition, we further examined the effect of

concentration of the HNO_3 solution on membrane structure and separation performance. Specifically, different concentration HNO_3 solution (i.e., 0.01, 0.1 and 1 %) was used to etch the TFC-Cu100 membrane, and the etched membranes are denoted as TFC-Cu100X0.01, TFC-Cu100X0.1, and TFC-Cu100X, respectively.

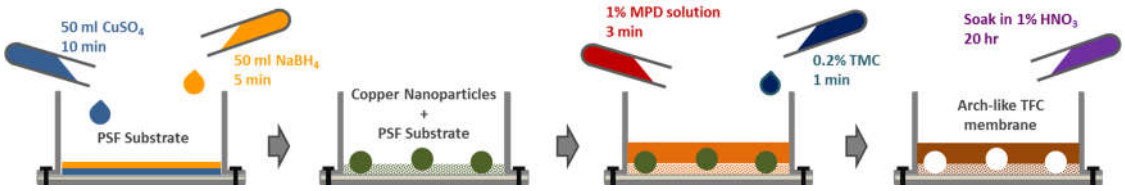

Fig.1. Fabrication scheme of the novel arch-like TFC membrane containing nanovoids. First, CuNPs were *in situ* generated onto polysulfone surface by the additional of $CuSO_4$ and $NaBH_4$ (50, 100 and 200 mM) respectively, followed by performing interfacial polymerization reaction between 1% MPD and 0.2% TMC. The resultant CuNPs contained membrane was then etched by 1% HNO_3 solution to obtain the final product membrane.

2.4. Membrane Characterization

Membrane surface morphology was examined by scanning electron microscopy (SEM, LEO 1530, UK) and the elemental composition of the membranes were analyzed by energy dispersive spectroscopy (EDS). Before the measurement, membranes samples were dried in air, coating with gold and platinum. SEM characterization was applied at an accelerating voltage of 5 kV, while EDS analysis was conducted at the voltage of 20 kV. Transmission electron microscopy (Philips CM100, TEM) was applied for analyzing the cross-sectional membrane morphology based on our previous method [23]. Substrate pore size and CuNPs size distribution were analyzed by image software (Image-Pro Plus, MediaCybernetics, Inc).

Attenuated total reflection Fourier transform infrared (ATR-FTIR, Nicolet 6700) spectroscopy was used to assess membrane functional groups over a wave number range from 650 to 4000 cm^{-1} at a resolution of 2 cm^{-1}. The roughness of membrane surface was determined by atomic force microscopy (AFM, Multimode 8, Bruker, MA) with a scanning size of 5 × 5 μm. The value of root-mean-square roughness (RMS or R_q) was obtained using software Nanoscope Analysis software (Bruker, MA).

2.5. Separation performance testing

A cross-flow laboratory filtration setup was used to test membrane water flux and salt rejection [24]. The membrane was first filtrated at an applied pressure of 21 bar for 3 hours with 2000 ppm NaCl solution as feed solution. Then, the pressure was set at 20 bar for the measurement of water flux. The water flux was determined based on the volume of permeate water collected over a specified time interval (Equation (1)). Membrane salt rejection (R) was calculated based on the measured conductivity of the feed solution and permeates water (Equation (2)) using an electric conductivity meter (Ultrameter II ^{TM}, model 4P, Myron Company, Carlsbad, CA).

$$J_w = \frac{\Delta V}{\Delta t \times A} \quad (1)$$

where J_w ($Lm^{-2}h^{-1}$) is the water flux, Δt (h) is the testing time, A (m^2) is the membrane area, ΔV (L) is the volume of permeate.

$$R = (1 - \frac{C_p}{C_f}) \times 100\% \quad (2)$$

where C_p is the conductivity of permeate and C_f is the conductivity of the original feed solution.

According to the solution-diffusion model [25], water permeability and salt permeability are calculated by Equation (3) and (4), respectively.

$$A = \frac{J_w}{\Delta P - \Delta \pi} \quad (3)$$

$$B = \frac{1 - R}{R} J_w \quad (4)$$

where A ($Lm^{-2}h^{-1}bar^{-1}$) is the membrane water permeability constant, B ($Lm^{-2}h^{-1}$) is the membrane salt permeability constant, ΔP is the applied pressure and $\Delta \pi$ is the osmotic pressure difference between feed and permeate solution.

2.6. Quantifying of copper loading

To measure the total amounts of copper in membrane samples, CuNPs incorporated membrane coupons (Membrane area=0.95 cm^2) was immersed in a strong acidic solution (0.2 ml 69% HNO_3 in 20 ml DI water) under 100 rpm for 3 days. The dissolved copper concentrations in the acidic leaching solutions were quantified by an inductive coupled plasma optical emission spectrometer (ICP-OES, Optima 8×00, PerkinElmer).

3. Results and discussion

3.1. Membrane characterization

Fig. 2 presents the SEM micrographs (plan view) of the control (PSF) and $CuSO_4/NaBH_4$ modified polysulfone (PSF-Cu) substrates. The control polysulfone substrate had a relatively flat surface with a root-mean-square (R_q) roughness of 9.3 ± 1.8 nm. With the increased concentration of the applied $CuSO_4$ and $NaBH_4$ solution, the surface roughness of the modified substrate increased up to 14.9 ± 3.4 nm (Supplementary material, Fig. A1). Elemental analysis of EDS (inserts of Fig. 2) further confirmed that the increased amounts of copper were generated on substrates. The increased roughness and the copper loading may be due to the formation of copper nanoparticles (CuNPs). Ben-Sasson and co-workers reported that the redox reaction between $CuSO_4$ and $NaBH_4$ led to the formation of uniform CuNPs of a few tens of nanometers. Further analysis suggests that the average size of the *in situ* generated CuNPs is 15.7 ± 4.8 nm (Fig. A4, CuNPs size distribution), which is comparable to that reported in the literature [22]. Substrate pore size significantly decreased from 35.2 ± 12.8 nm for the control PSF substrate to 17.6 ± 4.7 nm for the PSF-Cu200 substrate as a result of CuNPs loading. In addition, the PSF-Cu200 substrate showed an increased contact angle of 91.4 ± 2.3° compared to that of the control PSF substrate (83.3 ± 1.7°, Table A1). This shift in contact angle value is consistent with the existing literature reporting a more hydrophobic surface after the *in situ* reaction between $NaBH_4$ and $CuSO_4$ [22].

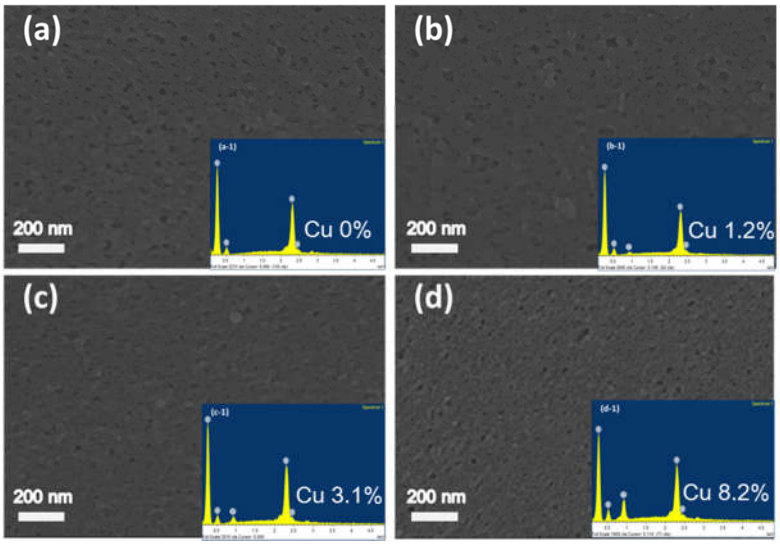

Fig.2. SEM micrographs of (a) control PSF, (b) PSF-Cu50, (c) PSF-Cu100 and (d) PSF-Cu200 substrates. The corresponding EDS spectra and Cu mass loading are shown in the insert of each micrograph. The scale bar of all SEM micrographs is 200 nm.

Interfacial polymerization was performed on the PSF and PSF-Cu substrates to prepare the control membrane (TFC) and the copper loaded polyamide membranes (TFC-Cu), respectively. These TFC-Cu membranes were subsequently treated by 1% HNO_3 solution to etch away the CuNPs in the polyamide membranes (TFC-CuX). Fig. 3a and B2 show the surface morphology of these membranes. The control TFC and all TFC-Cu membranes exhibited ridge-and-valley roughness features that are commonly observed for the MPD/TMC interfacial chemistry [26]. Even though CuNPs cannot be directly observed noting that they were covered by the polyamide layer, EDS analysis (Fig. 3b) confirmed their presence thanks to the relatively deep sample penetration depth of several micrometers [27]. Furthermore, the surface roughness of the TFC-Cu membranes systematically increased from 38.8 ± 8.4 nm of the control TFC to 58.4 ± 2.6 nm of TFC-Cu200 membrane (Supplementary material, Fig. A2), potentially due

to the embedded CuNPs underneath the polyamide layer [24, 28]. Compared to TFC-Cu membranes, the membranes etched by 1% HNO_3 (TFC-CuX) showed no significant changes in the surface morphology (Fig. 3a) and FTIR spectra (Supplementary material, Fig. B1). Nevertheless, the characteristic dark color of the CuNPs loaded membranes disappeared after the acid treatment (inserts of Fig. 3b). Both EDX (Fig. 3b) and ICP results (Fig. 3c) show that the residual amount of copper in the TFC-CuX membranes were negligible, confirming the successful removal of CuNPs by the 1% HNO_3 treatment.

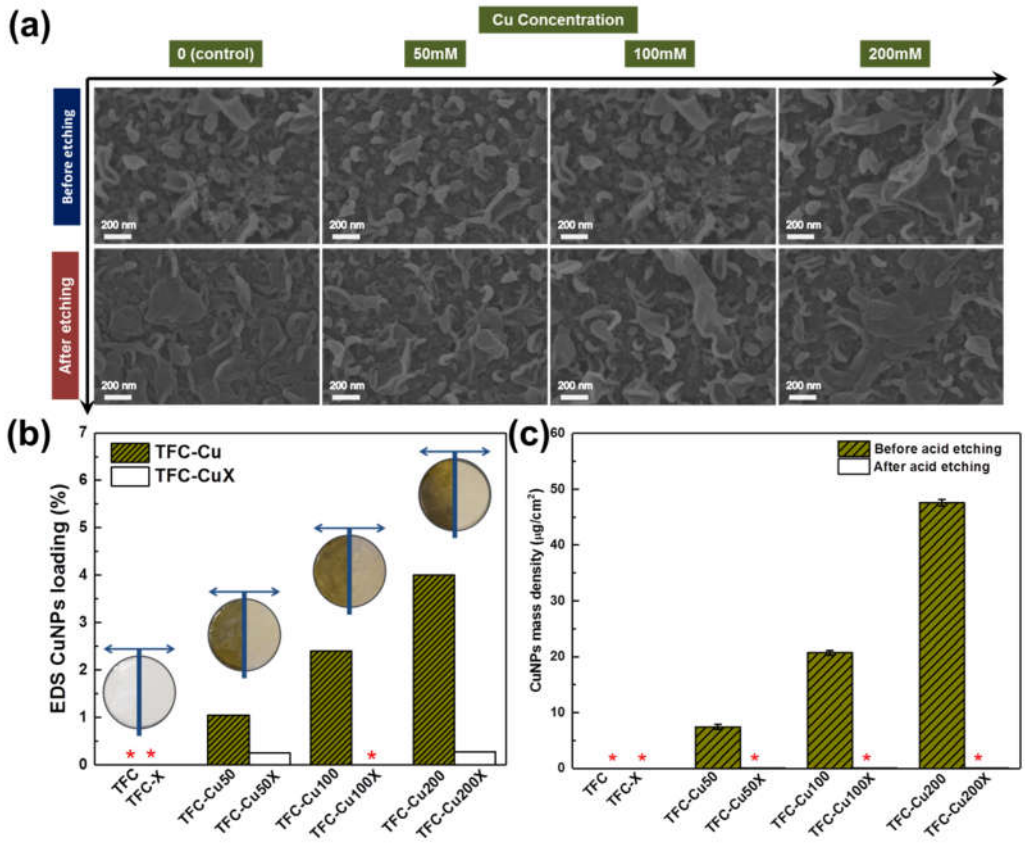

Fig. 3. Characterization of TFC, TFC-Cu, and TFC-CuX membranes. (a) SEM micrographs. The

Upper panel shows the control TFC and the CuNPs embedded TFC membranes (TFC-Cu50, TFC-Cu100 and TFC-Cu200), while the lower panel shows the corresponding HNO_3 solution etched membranes (TFC-X, TFC-Cu50X, TFC-Cu100X and TFC-Cu200X membranes). The scale bar for all SEM micrographs is 200 nm. (b) CuNPs mass loading analyzed by EDS and the digital photos of the membranes before (left-hand side) and after (right-hand side) HNO_3 etching. (c) ICP CuNPs mass density results of all membranes. Symbol * stands for below detection limit.

We further analyzed the effect of HNO_3 solution concentration on the degree of etching using TFC-Cu100 membranes. Whereas the etched TFC-Cu100X membranes exhibited similar morphologies (Fig. 4a), their color became progressively lighter (inserts of Fig. 4b) as the concentration of HNO_3 significantly increased from 0.01 to 1%. This reveals the process from partial to fully etching of the CuNPs at higher HNO_3 concentration, which is further confirmed by the mass loading (EDS analysis, Fig. 4b) and density (ICP results, Fig. 4c) of copper. Notably, when the concentration of HNO_3 increased to 1 wt. %, the CuNPs mass loading of the TFC-Cu100 membrane was below the detection limit, indicating the complete removal of CuNPs.

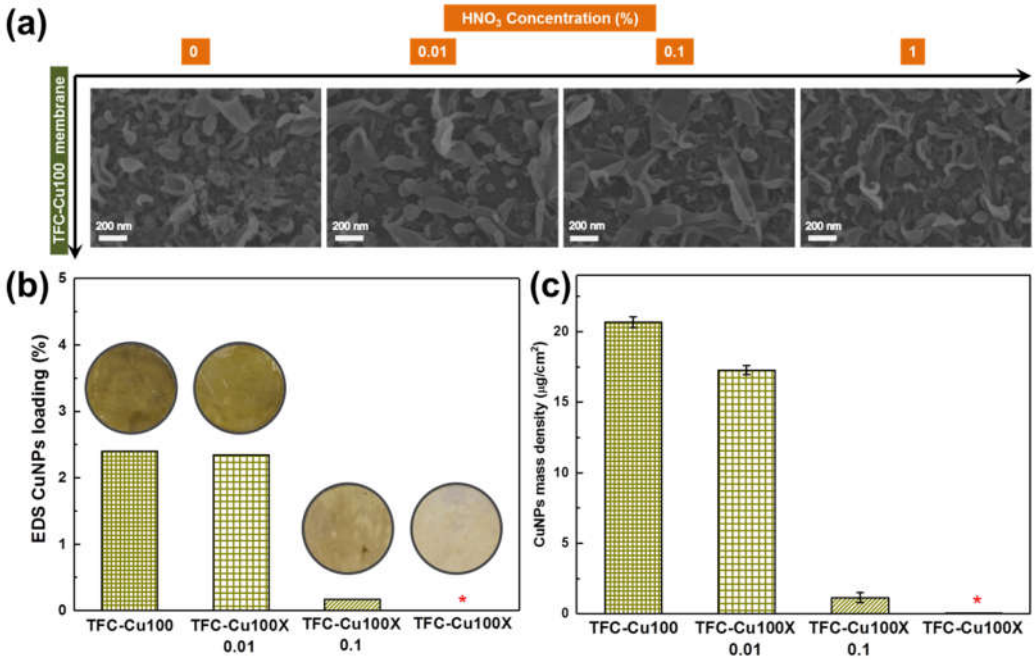

Fig. 4. Effect of HNO_3 concentration on copper etching. (a) SEM micrographs of TFC-Cu100 membrane treated by different concentration of the HNO_3 solution (0.01, 0.1 and 1 wt. %). Effect of HNO_3 concentration on copper etching. (b) EDS analysis of CuNPs mass loading and the digital photos of the TFC-Cu100 and TFC-Cu100X membranes. (c) ICP results of CuNPs mass density results of the TFC-Cu100 and TFC-Cu100X membranes. Symbol * stands for below detection limit.

Fig. 5 presents the TEM cross-sectional images of the TFC-Cu100 (without etching) and the TFC-Cu100X membranes (etched at 0.01, 0.1, and 1% HNO_3, respectively). Compared to the control TFC-Cu100 membrane (Fig. 5a), the TFC-Cu100X membranes (Fig. 5b-d) showed an increasing number of nanovoids as the concentration of HNO_3 solution increased from 0.01 to 1%. These nanovoids, whose dimension was on the order of 10 nm (comparable to the size of the CuNPs of 15.7 ± 4.8 nm), can be attributed to the removal of the CuNPs in the PA-PSF interface, as confirmed by the EDS and ICP results (Fig. 4b,c). Additional TEM cross-sectional micrographs of TFC-Cu50X and TFC-Cu200X membranes are presents in Fig. B4.

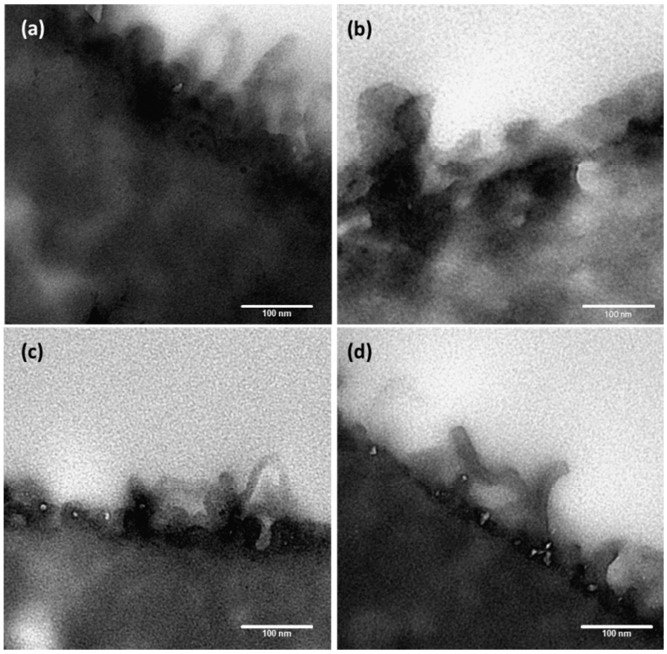

Fig. 5 TEM cross-sectional images of the (a) TFC-Cu100 (a) and (b-d) TFC-Cu100X membranes etched at 0.01, 0.1 and 1% HNO_3 solution, respectively. The scale bar for all TEM micrographs is 100 nm.

3.2. Membrane separation performances

Fig. 6 presents membrane separation performance of the membranes. The control TFC membrane had a water flux of 15.1 ± 0.5 $Lm^{-2}h^{-1}$ and NaCl rejection of 96.7 ± 0.3% at an applied pressure of 20 bar (Fig. 6). Acid treatment by 1% HNO_3 had no apparent impact on its separation properties, indicating that the polyamide rejection layer was not compromised in the strong acid [29]. With the incorporation of CuNPs in the polyamide rejection layer, the water fluxes of TFC-Cu membranes were approximately halved compared to that of the control TFC membrane. The increased hydraulic resistances of the TFC-Cu membranes were caused by the presence of the solid CuNPs, which blocks the passage of water molecules. In addition, the decreased

surface pore size and hydrophilicity of the CuNPs loaded PSF substrate may also be partially responsible for the reduced water flux of the corresponding TFC-Cu membranes [30, 31]. Similar observations have been reported by Zhao et al., [32], who found that the incorporation of impermeable lipid vesicles in polyamide rejection layers caused a reduced membrane permeability

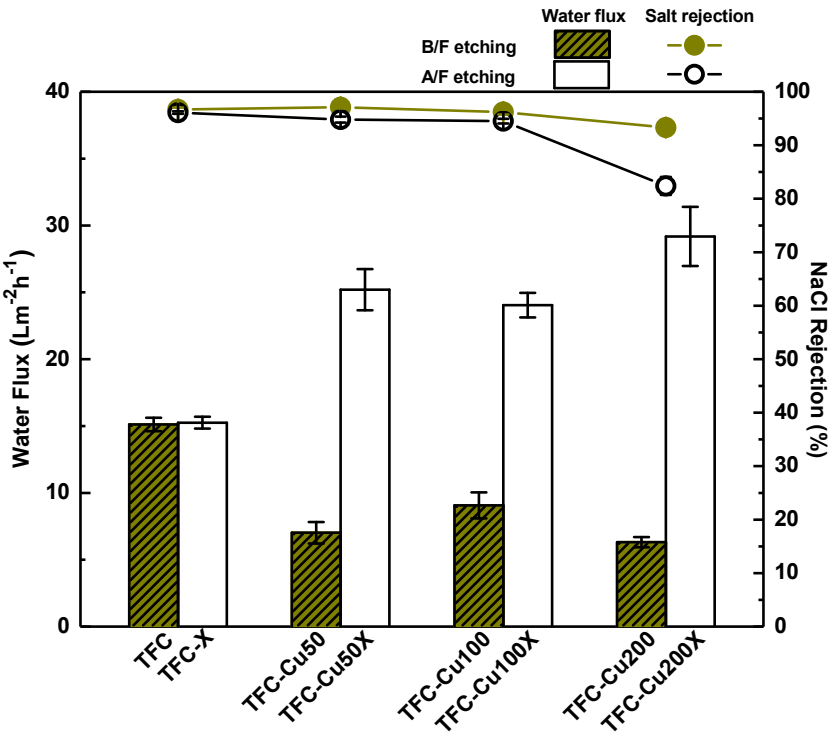

Fig. 6. Membrane separation performance (water flux and salt rejection) of the control TFC-Cu50, TFC-Cu100, and TFC-Cu200 membranes before and after etching by 1% HNO_3 solution. The separation performance was evaluated using a feed solution of 2000 ppm NaCl at 20 bar.

After etching, the water flux of the TFC-CuX membrane was significantly improved compared to that of the corresponding TFC-Cu membrane (Fig. 6). For example, the TFC-Cu50X membrane had a water flux of 25.2 ± 1.5 $Lm^{-2}h^{-1}$, which was nearly 300%

299 higher than that of the TFC-Cu50 membrane of 7.0 ± 0.8 $Lm^{-2}h^{-1}$. The significantly
300 enhanced water flux can be attributed to the creation of additional nanovoids in the
301 dense polyamide layer, thus providing additional shortcuts for water transport.
302 Compared to the control TFC membrane, the TFC-Cu50X membrane achieved a 70%
303 enhancement in water flux while maintaining similar NaCl rejection. Although more
304 permeable membranes can be prepared by loading greater amount of CuNPs followed
305 by their subsequent removal, overloading CuNPs and their subsequent etching can
306 lead to a loss of rejection. In particular, the TFC-Cu200X membrane had a NaCl
307 rejection of only 82.4 ± 1.7%, which was substantially lower than that of the control
308 TFC (96.7 ± 0.4%). The extensive nanovoids generated in the TFC-Cu200X
309 membrane after HNO_3 etching could have jeopardized the integrity of the polyamide
310 rejection layer.
311
312 The effect of pressure on membrane separation test was conducted by measuring
313 membrane water flux and NaCl rejection over an applied pressure range of 10-25 bar
314 (Fig. 7). The etched membranes (TFC-Cu50X, TFC-100CuX, and TFC-200CuX),
315 even though containing nanovoids in their rejection layer after HNO_3 treatment,
316 showed a linear relationship between water flux and applied pressure, which is
317 consistent with other literature [33, 34]. Furthermore, their NaCl rejection (Fig. 7 b,d)
318 significantly improved as the applied pressure increased. These results are in good
319 agreement with the solution-diffusion theory [25].

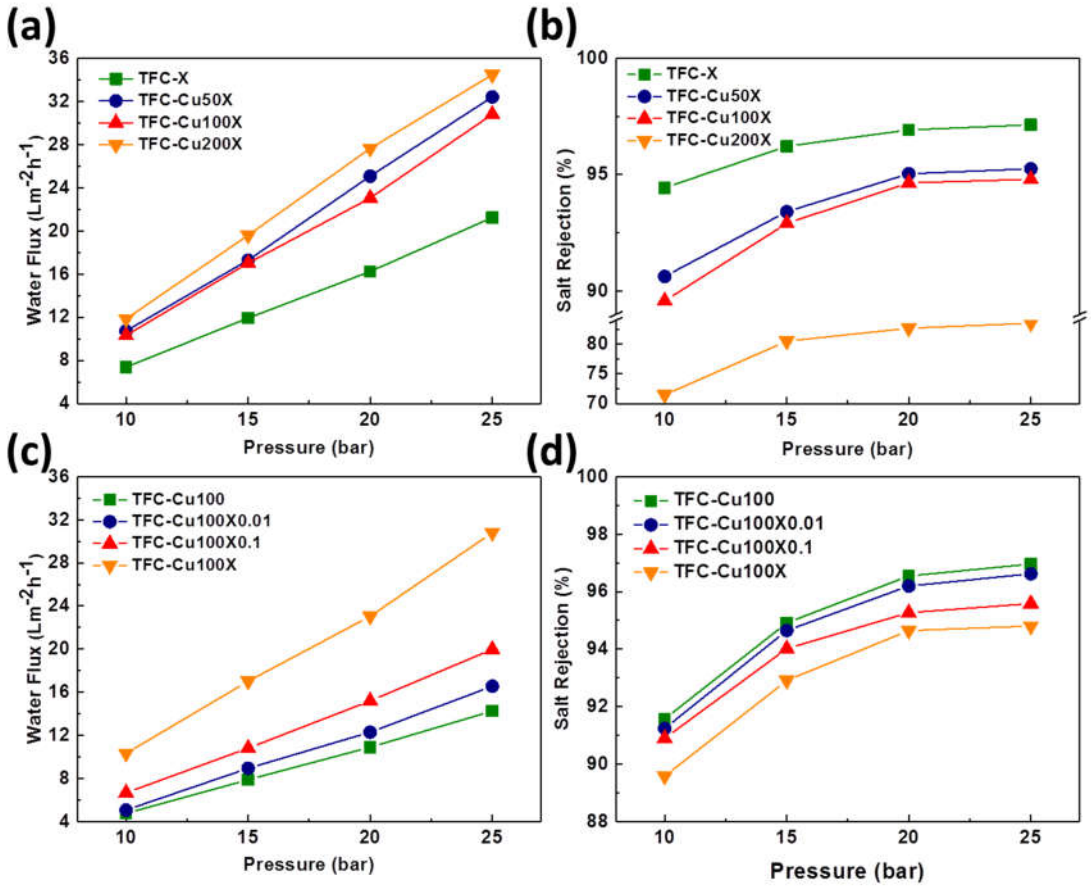

Fig. 7 Membrane separation tests under different applied pressures (10-25 bar). Water flux and NaCl rejection of all etched membranes of the TFC-X and TFC-Cu50/100/200X membranes (a-b), and the TFC-Cu100 and TFC-Cu100X that were etched by different concentration HNO_3 solution (c-d). All presented data are based on the average value of three parallel membrane samples.

3.3. Comparison to conventional TFN membranes

Table 1 summarizes the recently published TFN membranes in accordance with the nanomaterials incorporated, their loading amounts, and the impact on the separation performance. In general, these TFN membranes were fabricated by incorporating certain amounts of porous nanomaterials (with characteristic pore or channel size on the order of 0.1-10 nm) either in aqueous (MPD) or organic (TMC) phase during the

interfacial polymerization reaction. In many cases, the water flux improved (up to 200%) as a result of loading these nanoporous materials in the polyamide rejection layer, which was accompanied with either decreased or similar NaCl rejection. Specifically, in some cases, the incorporation of mesoporous silica [7], MWCNTs [9] and GO [35] with relatively large pore size or interlayer spacing (i.e., with characteristic pores size up to several nm), may lead to the loss of NaCl rejection associated with significantly enhanced water flux. This can be potentially due to the deteriorated polyamide integrity or the oversized pores that simultaneously increase both water molecules and solutes transport [1]. On the other hand, when the pore size is relatively small, such as MOFs of 0.6 nm [36] and aquaporin of 0.3 nm [32], their corresponding TFN membranes have similar NaCl rejection with marginally improved water flux compared to that of the control. Notably, one study [37] on aquaporin incorporated TFN membranes showed both enhanced water flux and salt rejection, thanks to the highly permeable and selective channels of aquaporin [38-43].

In the current study, we synthesized nanovoids-enhanced TFC membranes by etching the CuNPs-based TFN membranes. Compared to the TFN membranes without etching, the nanovoids-enhanced approach offers additional pathways for water transport and thus improves membrane water flux. For example the etched membrane TFC-Cu50X showed approximately 260% higher water flux compared to the membrane TFC-Cu50 without etching, revealing the important role of nanovoids in facilitating water

transport. This membrane also had a 70% higher water flux compared to that of the control TFC membrane while maintaining similar NaCl rejection. This approach opens new possibilities of preparing high permeability desalination membranes. Though the current CuNPs-based approach is somewhat complicated, this method can be potentially extended to other more soluble nanomaterials, such as MOFs [44, 45], to eliminate the need for the acid etching. The NaCl rejection of the nanovoids-containing TFC membrane is slightly lower than that of the control and TFC-Cu membranes and it is within the traditional flux-rejection trade-off. A comparison of the nanovoids-containing TFC membranes with commercial RO membranes (Table B1) also suggests the need to further enhance their NaCl rejection. Considering the critical role of size effect (Table 1), future studies should consider the optimization of the properties of the nanovoids (e.g., size, number density, etc.) in addition to the further tuning of reaction conditions of interfacial polymerization [3].

368 Table 1. Comparison of recent thin-film nanocomposite reverse osmosis membranes to this work.

Nanofiller	Pore size (nm)	Polymer	Optimal loading (%)	Performance	Published year and Reference
Nanovoids	~10	PA[a]	~8 μg/cm^2 CuNPs etched by 1% HNO_3	Pw ↑ by 70% with slightly ↓ NaCl rejection compared to TFC Pw ↑ by 260% with slightly ↓ NaCl rejection compared to TFC-Cu	This work
Zeolite	~0.4	PA	0.4% (w/v) in organic phase	Pw ↑ by 81% with slightly ↓ NaCl rejection	2007 [4]
Zeolite	~0.4	PA	0.2% (w/v) in organic phase	Pw ↑ by 47% with slightly ↓ NaCl rejection	2009 [5]
Mesoporous silica	~3	PA	0.05 (w/v) in organic phase	Pw ↑ by 64%; No change in NaCl rejection	2012 [6]
Mesoporous silica	~2.5	PA	0.1 (w/v) in organic phase	P_w ↑ by 180% with slightly ↓ NaCl rejection	2013 [7]
Micro/Mesoporous silica	~1.8/~2.5	PA	0.05 (w/v) in organic phase	P_w ↑ by 41%; No change in NaCl rejection	2016 [46]
Proteoliposome with aquaporin	~0.3	PA	10 mgmL^{-1} in aqueous phase	P_w ↑ by 25%; No change in NaCl rejection	2012 [32]
Proteoliposome with aquaporin	~0.3	PA	Not available	P_w ↑ by 90%; ↑ NaCl rejection	2016 [37]
MOFs[b]	~3.4	PA	0.2 (w/v) in organic phase	Flux ↑ by 130% with similar solvent rejection	2013 [8]
MOFs	~0.6	PA	0.1 (w/v) in organic phase	P_w ↑ by 52%; No change in NaCl rejection	2017 [36]
MWCNTs[c]	~5	PA	0.1 (w/v) in aqueous phase	P_w ↑ by 80% with ↓↓ NaCl rejection	2014 [9]
MWCNTs-NH_2	~5-20	PA	0.003 (w/v) in aqueous phase	Pw ↑ by 38%; No change in NaCl rejection	2017 [47]
GO[d]	-	PA	~40 ppm in aqueous phase	Pw ↑ by 84%; No change in NaCl rejection	2015 [48]
GO	0.83 interlayer space	PA	0.02% (w/v) in organic phase	Pw ↑ by 52% with slightly ↓ NaCl rejection	2016 [35]

369 Note:

370 [a] PA: polyamide

371 [b] MOFs: metal-organic frameworks

372 [c] MWCNTs: Multi-walled carbon nanotubes

373 [d] GO: graphene oxide

374 Adapted from Ref. [24]

375

3.4. Conclusions

In this study, novel nanovoids-enhanced TFC membranes were fabricated by etching CuNPs incorporated in the PA-PSF interface using a strong acid. The resulting etched TFC-CuX membranes showed significantly improved water permeability compared to both the control TFC membrane and the corresponding CuNPs containing counterpart. Our study clearly demonstrates the feasibility of using sacrificial CuNPs in creating nanovoids as well as their critical role in enhancing water transport through the polyamide rejection layer. Future study may further explore the impact of the nanovoids sizes and density on membrane separation performance as well as alternative candidates of removable nanomaterials.

Acknowledgement

This study receives financial support from the Seed Funding for Strategic Interdisciplinary Research Scheme, the University of Hong Kong.

Appendices

Appendix A. AFM, ATR-FTIR and contact angle results of all substrates and CuNPs size distribution; Appendix B. ATR-FTIR, additional SEM and TEM, separation performance, a table of comparison of commercial membranes to this work.

References

[1] J. Yin, B. Deng, Polymer-matrix nanocomposite membranes for water treatment, J. Membr. Sci., 479 (2015) 256-275.

[2] W. Lau, S. Gray, T. Matsuura, D. Emadzadeh, J.P. Chen, A. Ismail, A review on polyamide thin film nanocomposite (TFN) membranes: History, applications, challenges and approaches, Water Res., 80 (2015) 306-324.

[3] D. Li, Y. Yan, H. Wang, Recent advances in polymer and polymer composite membranes for reverse and forward osmosis processes, Prog. Polym. Sci., 61 (2016) 104-155.

[4] B.-H. Jeong, E.M. Hoek, Y. Yan, A. Subramani, X. Huang, G. Hurwitz, A.K. Ghosh, A. Jawor, Interfacial polymerization of thin film nanocomposites: a new concept for reverse osmosis membranes, J. Membr. Sci., 294 (2007) 1-7.

[5] M.L. Lind, A.K. Ghosh, A. Jawor, X. Huang, W. Hou, Y. Yang, E.M. Hoek, Influence of zeolite crystal size on zeolite-polyamide thin film nanocomposite membranes, Langmuir, 25 (2009) 10139-10145.

[6] J. Yin, E.-S. Kim, J. Yang, B. Deng, Fabrication of a novel thin-film nanocomposite (TFN) membrane containing MCM-41 silica nanoparticles (NPs) for water purification, J. Membr. Sci., 423 (2012) 238-246.

[7] M. Bao, G. Zhu, L. Wang, M. Wang, C. Gao, Preparation of monodispersed spherical mesoporous nanosilica–polyamide thin film composite reverse osmosis membranes via interfacial polymerization, Desalination, 309 (2013) 261-266.

[8] S. Sorribas, P. Gorgojo, C. Téllez, J. Coronas, A.G. Livingston, High flux thin film nanocomposite membranes based on metal–organic frameworks for organic solvent nanofiltration, J. Am. Chem. Soc., 135 (2013) 15201-15208.

[9] H. Zhao, S. Qiu, L. Wu, L. Zhang, H. Chen, C. Gao, Improving the performance of polyamide reverse osmosis membrane by incorporation of modified multi-walled carbon nanotubes, J. Membr. Sci., 450 (2014) 249-256.

[10] Z. Yang, X.-H. Ma, C.Y. Tang, Recent development of novel membranes for desalination, Desalination, (2017).

[11] M.L. Lind, D. Eumine Suk, T.-V. Nguyen, E.M. Hoek, Tailoring the structure of thin film nanocomposite membranes to achieve seawater RO membrane performance, Environ. Sci. Technol., 44 (2010) 8230-8235.

[12] L. Lin, R. Lopez, G.Z. Ramon, O. Coronell, Investigating the void structure of the polyamide active layers of thin-film composite membranes, J. Membr. Sci., 497 (2016) 365-376.

[13] X.-H. Ma, Z.-K. Yao, Z. Yang, H. Guo, Z.-L. Xu, C.Y. Tang, M. Elimelech, Nanofoaming of polyamide desalination membranes to tune permeability and selectivity, Environ. Sci. Technol. Lett., 5 (2018) 123-130.

[14] M.F. Jimenez-Solomon, Q. Song, K.E. Jelfs, M. Munoz-Ibanez, A.G. Livingston, Polymer nanofilms with enhanced microporosity by interfacial polymerization, Nat. Mater., 15 (2016) 760.

[15] Q. An, W.-S. Hung, S.-C. Lo, Y.-H. Li, M. De Guzman, C.-C. Hu, K.-R. Lee, Y.-C. Jean, J.-Y. Lai, Comparison between free volume characteristics of composite membranes fabricated through static and dynamic interfacial polymerization processes, Macromolecules, 45 (2012) 3428-3435.
[16] C. Kong, T. Kamada, T. Shintani, M. Kanezashi, T. Yoshioka, T. Tsuru, Enhanced performance of inorganic-polyamide nanocomposite membranes prepared by metal-alkoxide-assisted interfacial polymerization, J. Membr. Sci., 366 (2011) 382-388.
[17] C. Kong, M. Kanezashi, T. Yamomoto, T. Shintani, T. Tsuru, Controlled synthesis of high performance polyamide membrane with thin dense layer for water desalination, J. Membr. Sci., 362 (2010) 76-80.
[18] F.A. Pacheco, I. Pinnau, M. Reinhard, J.O. Leckie, Characterization of isolated polyamide thin films of RO and NF membranes using novel TEM techniques, J. Membr. Sci., 358 (2010) 51-59.
[19] J. Liu, D. Hua, Y. Zhang, S. Japip, T.S. Chung, Precise molecular sieving architectures with Janus pathways for both polar and nonpolar molecules, Adv. Mater., 30 (2018) 1705933.
[20] S. Xiong, D.Y. Zhang, S. Mei, J. Liu, Y.S. Shi, Y. Wang, Thin film composite membranes containing intrinsic CD cavities in the selective layer, J. Membr. Sci., 551 (2018) 294-304.
[21] X.-H. Ma, Z. Yang, Z.-K. Yao, Z.-L. Xu, C.Y. Tang, A facile preparation of novel positively charged MOF/chitosan nanofiltration membranes, J. Membr. Sci., 525 (2017) 269-276.
[22] M. Ben-Sasson, X. Lu, S. Nejati, H. Jaramillo, M. Elimelech, In situ surface functionalization of reverse osmosis membranes with biocidal copper nanoparticles, Desalination, 388 (2016) 1-8.
[23] Z. Yang, Y. Wu, J. Wang, B. Cao, C.Y. Tang, In situ reduction of silver by polydopamine: A novel antimicrobial modification of a thin-film composite polyamide membrane, Environ. Sci. Technol., 50 (2016) 9543-9550.
[24] Z. Yang, Y. Wu, H. Guo, X.-H. Ma, C.-E. Lin, Y. Zhou, B. Cao, B.-K. Zhu, K. Shih, C.Y. Tang, A novel thin-film nano-templated composite membrane with in situ silver nanoparticles loading: Separation performance enhancement and implications, J. Membr. Sci., 544 (2017) 351-358.
[25] G.M. Geise, H.B. Park, A.C. Sagle, B.D. Freeman, J.E. McGrath, Water permeability and water/salt selectivity tradeoff in polymers for desalination, J. Membr. Sci., 369 (2011) 130-138.
[26] A.K. Ghosh, B.-H. Jeong, X. Huang, E.M. Hoek, Impacts of reaction and curing conditions on polyamide composite reverse osmosis membrane properties, J. Membr. Sci., 311 (2008) 34-45.
[27] M.P. Seah, W. Dench, Quantitative electron spectroscopy of surfaces: A standard data base for electron inelastic mean free paths in solids, Surf. Interf. Anal., 1 (1979) 2-11.

[28] L.-x. Dong, X.-c. Huang, Z. Wang, Z. Yang, X.-m. Wang, C.Y. Tang, A thin-film nanocomposite nanofiltration membrane prepared on a support with in situ embedded zeolite nanoparticles, Sep. Purif. Technol., 166 (2016) 230-239.
[29] D. Li, H. Wang, Recent developments in reverse osmosis desalination membranes, J. Mater. Chem., 20 (2010) 4551-4566.
[30] S. Xiong, J. Zuo, Y.G. Ma, L. Liu, H. Wu, Y. Wang, Novel thin film composite forward osmosis membrane of enhanced water flux and anti-fouling property with N-[3-(trimethoxysilyl) propyl] ethylenediamine incorporated, J. Membr. Sci., 520 (2016) 400-414.
[31] X. Zhang, L. Shen, W.-Z. Lang, Y. Wang, Improved performance of thin-film composite membrane with PVDF/PFSA substrate for forward osmosis process, J. Membr. Sci., 535 (2017) 188-199.
[32] Y. Zhao, C. Qiu, X. Li, A. Vararattanavech, W. Shen, J. Torres, C. Helix-Nielsen, R. Wang, X. Hu, A.G. Fane, Synthesis of robust and high-performance aquaporin-based biomimetic membranes by interfacial polymerization-membrane preparation and RO performance characterization, J. Membr. Sci., 423 (2012) 422-428.
[33] J. Fang, B. Deng, Arsenic rejection by nanofiltration membranes: effect of operating parameters and model analysis, Environ. Eng. Sci., 31 (2014) 496-506.
[34] Y.-y. Zhao, F.-x. Kong, Z. Wang, H.-w. Yang, X.-m. Wang, Y.F. Xie, T.D. Waite, Role of membrane and compound properties in affecting the rejection of pharmaceuticals by different RO/NF membranes, Front. Environ. Sci. En., 11 (2017) 20.
[35] J. Yin, G. Zhu, B. Deng, Graphene oxide (GO) enhanced polyamide (PA) thin-film nanocomposite (TFN) membrane for water purification, Desalination, 379 (2016) 93-101.
[36] D. Ma, S.B. Peh, G. Han, S.B. Chen, Thin-Film Nanocomposite (TFN) Membranes Incorporated with Super-Hydrophilic Metal–Organic Framework (MOF) UiO-66: Toward Enhancement of Water Flux and Salt Rejection, ACS Appl. Mater. Interfaces, 9 (2017) 7523-7534.
[37] S. Qi, R. Wang, G.K.M. Chaitra, J. Torres, X. Hu, A.G. Fane, Aquaporin-based biomimetic reverse osmosis membranes: Stability and long term performance, J. Membr. Sci., 508 (2016) 94-103.
[38] P. Agre, Aquaporin water channels, Biosci. Rep., 24 (2004) 127-163.
[39] Y.-x. Shen, P.O. Saboe, I.T. Sines, M. Erbakan, M. Kumar, Biomimetic membranes: a review, J. Membr. Sci., 454 (2014) 359-381.
[40] C. Tang, Y. Zhao, R. Wang, C. Hélix-Nielsen, A. Fane, Desalination by biomimetic aquaporin membranes: Review of status and prospects, Desalination, 308 (2013) 34-40.
[41] C. Tang, Z. Wang, I. Petrinić, A.G. Fane, C. Hélix-Nielsen, Biomimetic aquaporin membranes coming of age, Desalination, 368 (2015) 89-105.
[42] G. Sun, T.-S. Chung, K. Jeyaseelan, A. Armugam, Stabilization and

520 immobilization of aquaporin reconstituted lipid vesicles for water purification,
521 Colloids Surf., B, 102 (2013) 466-471.
522 [43] H.L. Wang, T.-S. Chung, Y.W. Tong, K. Jeyaseelan, A. Armugam, H.H.P. Duong,
523 F. Fu, H. Seah, J. Yang, M. Hong, Mechanically robust and highly permeable
524 AquaporinZ biomimetic membranes, J. Membr. Sci., 434 (2013) 130-136.
525 [44] J.-Y. Lee, Q. She, F. Huo, C.Y. Tang, Metal–organic framework-based porous
526 matrix membranes for improving mass transfer in forward osmosis membranes, J.
527 Membr. Sci., 492 (2015) 392-399.
528 [45] Z. Wang, Z. Wang, S. Lin, H. Jin, S. Gao, Y. Zhu, J. Jin, Nanoparticle-templated
529 nanofiltration membranes for ultrahigh performance desalination, Nat. Commun., 9
530 (2018) 2004.
531 [46] Z. Yang, J. Yin, B. Deng, Enhancing water flux of thin-film nanocomposite (TFN)
532 membrane by incorporation of bimodal silica nanoparticles, Aims Press Envrion. Sci.,
533 3 (2016) 185-198.
534 [47] V. Vatanpour, M. Safarpour, A. Khataee, H. Zarrabi, M.E. Yekavalangi, M.
535 Kavian, A thin film nanocomposite reverse osmosis membrane containing
536 amine-functionalized carbon nanotubes, Sep. Purif. Technol., 184 (2017) 135-143.
537 [48] H.-R. Chae, J. Lee, C.-H. Lee, I.-C. Kim, P.-K. Park, Graphene oxide-embedded
538 thin-film composite reverse osmosis membrane with high flux, anti-biofouling, and
539 chlorine resistance J. Membr. Sci., 483 (2015) 128-135.
540